Finite-Strain Modelling of Polymeric Materials

LIÈGE université Aerospace & Mechanical engineering

Samuel Van Hulle (s.vanhulle@uliege.be)

Contents

1 Hyperelastic Material Models

1.1 Statistical Mechanics Approaches to Rubber Deformation

From the statistical mechanics approach of rubber elasticity [Treloar, 1975], rubber chain segments between chemical cross-links can be modeled as a number n rigid links of equal length l (Kuhn segments). The Freely Jointed Chain (FJC) model represents these chains by considering n rigid segments that are connected but freely hinged.

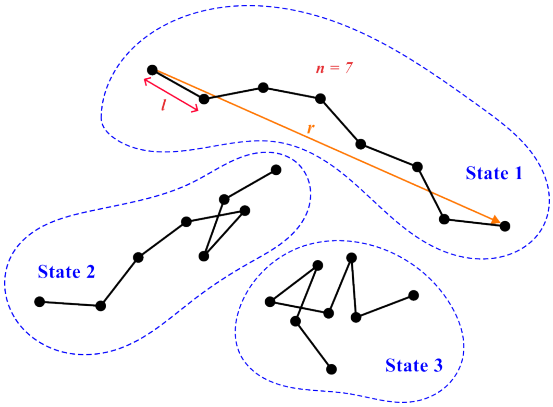

Fig. 1: Example of a FJC model with $n = 7$ segments and 3 possible deformation states.

A first statistical mechanics approach to describing the force on a deforming polymeric network assumed Gaussian statistics [Treloar, 1975], which states that the chains never approach their fully extent length r_{lock} given by

$$r_{lock} = nl. \tag{1}$$

From Gaussian statistics, the deviatoric part of the Helmholtz free energy writes

$$\psi' = C_1 \left(\bar{I}_1 - 3\right) = \frac{N k_B \theta}{2} \left(\bar{I}_1 - 3\right), \tag{2}$$

where N is the number of chains per unit reference volume, k_B is Boltzmann's constant and θ is the temperature.

Another statistical mechanics approach is the use of Langevin chain networks [Wang and Guth, 1952]. The initial chain length r_0 is taken from a random walk consideration of n steps with length l and writes [Arruda and Boyce, 1993]

$$r_0 = \sqrt{n} l, \tag{3}$$

so that the limiting extensibility, hence the chain locking stretch λ_{lock}, writes

$$\lambda_{lock} = \frac{r_{lock}}{r_0} = \sqrt{n}. \tag{4}$$

At any value of chain length r, the most probable angular distribution of rigid links may be found. Using Langevin statistics from Kuhn and Grün [1942], the probability distribution $\Omega(r)$

may be written in the logarithmic form as [Treloar, 1975]

$$\ln\left[\Omega(r)\right] = c - n\left(\frac{r}{nl}\mathcal{L}^{-1}\left[\frac{r}{nl}\right] + \ln\frac{\mathcal{L}^{-1}\left[\frac{r}{nl}\right]}{\sinh\,\mathcal{L}^{-1}\left[\frac{r}{nl}\right]}\right), \tag{5}$$

where c is a constant and $\mathcal{L}^{-1}$ is the inverse Langevin function, which will be discussed in a dedicated section. The entropy from a single chain η_{chain} can be determined from statistical mechanics [Reif, 1965] as

$$\eta_{chain} = k_B \ln\left[\Omega(r)\right] = k_B\left[c - n\left(\frac{r}{nl}\mathcal{L}^{-1}\left[\frac{r}{nl}\right] + \ln\frac{\mathcal{L}^{-1}\left[\frac{r}{nl}\right]}{\sinh\,\mathcal{L}^{-1}\left[\frac{r}{nl}\right]}\right)\right], \tag{6}$$

where k_B is Boltzmann's constant. Note that Langevin statistics properly accounts for the limiting chain extensibility, since $\mathcal{L}^{-1}\left[\frac{r}{nl}\right] \to \infty$ for $r \to r_{lock}$.

1.1.1 On the approximation of the inverse Langevin function

The Langevin function is defined by the following elementary functions

$$\mathcal{L}(x) = \coth(x) - \frac{1}{x}. \tag{7}$$

The inverse of this function has no explicit analytical form, but there exist several more or less precise approximations in the literature.

Arruda and Boyce [1993] have proposed to express the inverse Langevin function using the following five-term Taylor series expansion

$$\mathcal{L}^{-1}(x) \approx 3x + \frac{9}{5}x^3 + \frac{297}{175}x^5 + \frac{1539}{875}x^7 + \frac{126117}{67375}x^9, \tag{8}$$

which is only precise for $|x| < 0.5$.

Cohen [1991] proposes to approximate the inverse Langevin function using the Padé approximant

$$\mathcal{L}^{-1}(x) \approx x\frac{3 - x^2}{1 - x^2}, \tag{9}$$

which has a maximum relative error of 4.9% at $|x| = 0.8$.

Bergström [1999] proposes to separate the inverse Langevin function into two regions

$$\mathcal{L}^{-1}(x) \approx \begin{cases} 1.31446\,\tan(1.58986x) + 0.911209x, & \text{if } 0 \le |x| < 0.84136 \\ 1/(\text{sign}(x) - x), & \text{if } 0.84136 \le |x| < 1 \end{cases} \tag{10}$$

which has a relative error of 0.06% at $|x| = 0.7$.

Jedynak [2015] proposes the following expression for the inverse Langevin function

$$\mathcal{L}^{-1}(x) \approx x\frac{3 - 2.6x + 0.7x^2}{(1 - x)(1 + 0.1x)} \tag{11}$$

which has a maximum relative error of 1.5% for $|x| = 0.85$.

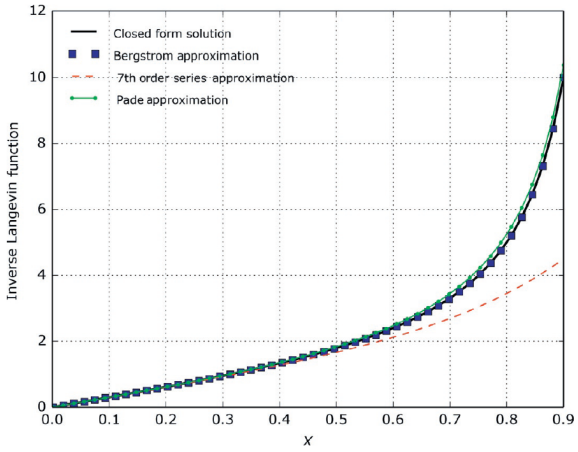

Fig. 2: Comparison between different approaches for calculating the inverse Langevin function [Bergström, 2015].

Note that other approximations also exist, but mostly to the detriment of computational efficiency. The choice of the implementation for the inverse Langevin function may seem to be a pointless issue but could lead to differences in the identification of material parameters depending on the FE software that is used. For example, Abaqus uses the five-term Taylor series expansion while the PolyUMod library (Ansys) uses the Bergström [1999] approximation.

1.2 The Eight-Chain Hyperelastic Model

The Eight-Chain (EC) model from Arruda and Boyce [1993], sometimes referred as the Arruda-Boyce model, is based on the deformation behavior of elastomer microstructures. The EC model assumes that chain molecules are, on average, located along the diagonal of a unit cell in the principal stretch space [Bergström, 2015].

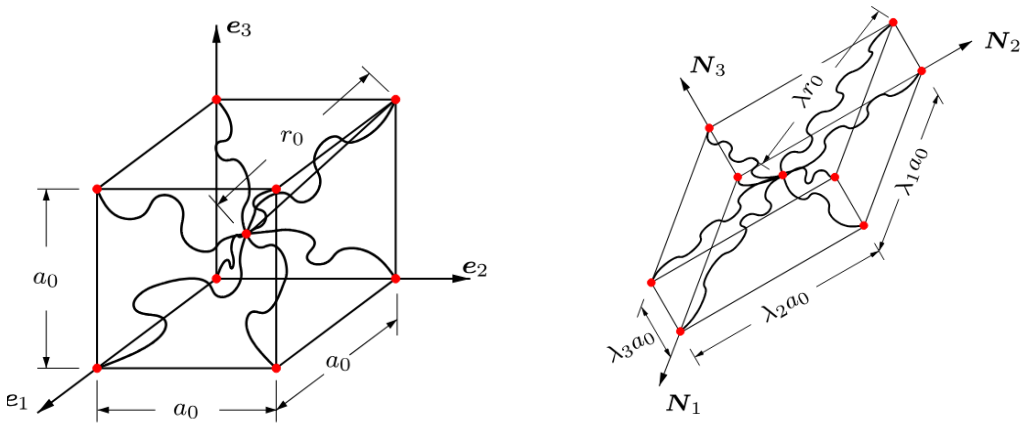

(a) **(b)**

Fig. 3: Eight-Chain model representation of the unit cell rubber network in the undeformed (a) and deformed (b) configuration [Dal and Kaliske, 2009].

The unstretched network includes eight chains of length $r_0 = \sqrt{n}l$ inside a cube of dimension

a_0, hence the following relation

$$a_0 = \frac{2}{\sqrt{3}} r_0. \tag{12}$$

Considering the application of principal distortional stretches λ_1^*, λ_2^* and λ_3^*, the chain length writes

$$r = \frac{a_0}{2}\sqrt{(\lambda_1^*)^2 + (\lambda_2^*)^2 + (\lambda_3^*)^2} = \frac{\sqrt{n}l}{\sqrt{3}}\sqrt{(\lambda_1^*)^2 + (\lambda_2^*)^2 + (\lambda_3^*)^2} = \frac{\sqrt{n\bar{I}_1}l}{\sqrt{3}} \tag{13}$$

and from there the effective distortional chain stretch writes

$$\bar{\lambda}^* = \frac{r}{r_0} = \sqrt{\frac{(\lambda_1^*)^2 + (\lambda_2^*)^2 + (\lambda_3^*)^2}{3}} = \sqrt{\frac{\mathrm{tr}\bar{\mathbf{C}}}{3}} = \sqrt{\frac{\mathrm{tr}\bar{\mathbf{B}}}{3}} = \sqrt{\frac{\bar{I}_1}{3}}, \tag{14}$$

showing that the distortional chain stretch is a function of the first invariant only. Based on this physically motivated model, the EC material is defined as an isotropic material whose Helmholtz free energy per unit reference volume ψ depends on two deformation invariants, $\bar{I}_1$ and J, and on the temperature θ_0. ψ can be determined using the experimental observation that for elastomers, the internal energy e_0 is typically not a function of the applied distortional chain stretch [Treloar, 1975] but only depends on the volume variation

$$\psi\left(\bar{\lambda}^*, J, \theta_0\right) = e_0\left(J\right) - \theta_0 \eta_0\left(\bar{\lambda}^*\right) = e_0\left(J\right) - \theta_0 N \eta_{chain}\left(\bar{\lambda}^*\right), \tag{15}$$

where N is the number of chains per unit reference volume. The assumption of small volume change has been used to avoid $\eta_0\left(\bar{\lambda}^*, J\right)$ and also ensures that the relationship between pressure and volumetric deformation is linear, hence

$$p = \frac{\boldsymbol{\sigma} : \mathbf{I}}{3} = \frac{\partial \psi}{\partial J} = k_0\left(J - 1\right), \tag{16}$$

where k_0 is the bulk modulus. Using the expression of η_{chain} and the relation $\frac{r}{nl} = \frac{\bar{\lambda}^*}{\sqrt{n}}$, the Helmholtz free energy finally writes

$$\psi\left(\bar{\lambda}^*, J, \theta_0\right) = N k_B \theta_0 n \left[\frac{\bar{\lambda}^*}{\sqrt{n}}\mathcal{L}^{-1}\left[\frac{\bar{\lambda}^*}{\sqrt{n}}\right] + \ln\left(\frac{\mathcal{L}^{-1}\left[\frac{\bar{\lambda}^*}{\sqrt{n}}\right]}{\sinh\,\mathcal{L}^{-1}\left[\frac{\bar{\lambda}^*}{\sqrt{n}}\right]}\right)\right] + \frac{k_0}{2}\left(J-1\right)^2. \tag{17}$$

The Cauchy stress for an Eight-Chain material can be obtained from continuum mechanics, which can be simplified since there is no dependence on $\bar{I}_2$ to

$$\begin{aligned}
\boldsymbol{\sigma} = \frac{2}{J}\mathbf{F}\frac{\partial \psi}{\partial \mathbf{C}}\mathbf{F}^T &= \frac{2}{J}\frac{\partial \psi}{\partial \bar{I}_1}\,\mathrm{dev}\left(\bar{\mathbf{B}}\right) + \frac{\partial \psi}{\partial J}\mathbf{I} = \frac{1}{J}\frac{1}{3\bar{\lambda}^*}\frac{\partial \psi}{\partial \bar{\lambda}^*}\,\mathrm{dev}\left(\bar{\mathbf{B}}\right) + \frac{\partial \psi}{\partial J}\mathbf{I} \\
&= \frac{-\theta_0 N}{3J\bar{\lambda}^*}\frac{\partial \eta_{chain}\left(\bar{\lambda}^*\right)}{\partial \bar{\lambda}^*}\,\mathrm{dev}\left(\bar{\mathbf{B}}\right) + k_0\left(J-1\right)\mathbf{I} \\
&= \frac{N k_B \theta_0}{3J}\frac{\sqrt{n}}{\bar{\lambda}^*}\mathcal{L}^{-1}\left(\frac{\bar{\lambda}^*}{\sqrt{n}}\right)\,\mathrm{dev}\left(\bar{\mathbf{B}}\right) + k_0\left(J-1\right)\mathbf{I}.
\end{aligned} \tag{18}$$

The expression for the Cauchy stress can be further simplified using the initial shear modulus

of the material, which is obtained for $\bar{I}_1 = 3$ hence, $\bar{\lambda^*} = 1$

$$\mu\left(\theta_0, N, \lambda^{lock}\right) = \frac{Nk_B\theta_0}{3}\lambda^{lock}\mathcal{L}^{-1}\left(\frac{1}{\lambda^{lock}}\right), \tag{19}$$

Using the shear modulus μ, the expression for the Cauchy stress simplifies to

$$\boldsymbol{\sigma} = \frac{\mu}{J\bar{\lambda^*}}\frac{\mathcal{L}^{-1}\left(\frac{\bar{\lambda^*}}{\lambda^{lock}}\right)}{\mathcal{L}^{-1}\left(\frac{1}{\lambda^{lock}}\right)}\,\mathrm{dev}\left(\bar{\mathbf{B}}\right) + k_0\left(J-1\right)\mathbf{I}, \tag{20}$$

which only depends on 3 material parameters μ, $\lambda^{lock} = \sqrt{n}$ and k_0.
An alternative expression can be encountered [Wu and van der Giessen, 1993] where the rubbery modulus C^R[MPa] is defined as

$$C^R = Nk_B\theta_0, \tag{21}$$

finally leading to the following expression of the Cauchy stress tensor

$$\boldsymbol{\sigma} = \frac{C^R}{3J}\frac{\lambda^{lock}}{\bar{\lambda^*}}\mathcal{L}^{-1}\left(\frac{\bar{\lambda^*}}{\lambda^{lock}}\right)\,\mathrm{dev}\left(\bar{\mathbf{B}}\right) + k_0\left(J-1\right)\mathbf{I}. \tag{22}$$

1.2.1 Example: the five-term Taylor series expansion

In their work, Arruda and Boyce [1993] use the five-term Taylor series expansion of the inverse Langevin function and obtain the following expression for the deviatoric part of the Helmholtz free energy

$$\psi' = Nk_B\theta_0\left[\frac{1}{2}\left(\bar{I}_1-3\right) + \frac{1}{20n}\left(\bar{I}_1^2-9\right) + \frac{11}{1050n^2}\left(\bar{I}_1^3-27\right) + \frac{19}{7000n^3}\left(\bar{I}_1^4-81\right) + \frac{519}{673750n^4}\left(\bar{I}_1^5-243\right)\right]. \tag{23}$$

From this expression, the deviatoric part of the Cauchy stress writes

$$\begin{aligned}\mathrm{dev}(\boldsymbol{\sigma}) &= \frac{2}{J}\frac{\partial\psi}{\partial\bar{I}_1}\,\mathrm{dev}\left(\bar{\mathbf{B}}\right)\\ &= \frac{2Nk_B\theta_0}{J}\left[\frac{1}{2} + \frac{1}{20n}2\bar{I}_1 + \frac{11}{1050n^2}3\bar{I}_1^2 + \frac{19}{7000n^3}4\bar{I}_1^3 + \frac{519}{673750n^4}5\bar{I}_1^4\right]\,\mathrm{dev}\left(\bar{\mathbf{B}}\right)\\ &= \frac{Nk_B\theta_0}{J}\left[1 + \frac{1}{5n}\bar{I}_1 + \frac{11}{175n^2}\bar{I}_1^2 + \frac{19}{875n^3}\bar{I}_1^3 + \frac{519}{67375n^4}\bar{I}_1^4\right]\,\mathrm{dev}\left(\bar{\mathbf{B}}\right).\end{aligned} \tag{24}$$

The same expression can be obtained starting from the expression of the Cauchy stress defined herebefore

$$\mathrm{dev}(\boldsymbol{\sigma}) = \frac{Nk_B\theta_0}{3J}\frac{\sqrt{n}}{\bar{\lambda^*}}\mathcal{L}^{-1}\left(\frac{\bar{\lambda^*}}{\sqrt{n}}\right)\,\mathrm{dev}\left(\bar{\mathbf{B}}\right), \tag{25}$$

and using the five-term Taylor series expansion of the inverse Langevin function

$$
\begin{aligned}
\mathrm{dev}(\boldsymbol{\sigma}) &= \frac{Nk_B\theta_0}{3J}\frac{\sqrt{n}}{\bar{\lambda}^*}\left[3\frac{\bar{\lambda}^*}{\sqrt{n}} + \frac{9}{5}\left(\frac{\bar{\lambda}^*}{\sqrt{n}}\right)^3 + \frac{297}{175}\left(\frac{\bar{\lambda}^*}{\sqrt{n}}\right)^5 + \frac{1539}{875}\left(\frac{\bar{\lambda}^*}{\sqrt{n}}\right)^7 + \frac{126117}{67375}\left(\frac{\bar{\lambda}^*}{\sqrt{n}}\right)^9\right] \mathrm{dev}\left(\bar{\mathbf{B}}\right) \\
&= \frac{Nk_B\theta_0}{J}\left[1 + \frac{3}{5}\left(\frac{\bar{\lambda}^*}{\sqrt{n}}\right)^2 + \frac{99}{175}\left(\frac{\bar{\lambda}^*}{\sqrt{n}}\right)^4 + \frac{513}{875}\left(\frac{\bar{\lambda}^*}{\sqrt{n}}\right)^6 + \frac{42039}{67375}\left(\frac{\bar{\lambda}^*}{\sqrt{n}}\right)^8\right] \mathrm{dev}\left(\bar{\mathbf{B}}\right) \\
&= \frac{Nk_B\theta_0}{J}\left[1 + \frac{3}{5n}\left(\sqrt{\frac{\bar{I}_1}{3}}\right)^2 + \frac{99}{175n^2}\left(\sqrt{\frac{\bar{I}_1}{3}}\right)^4 + \frac{513}{875n^3}\left(\sqrt{\frac{\bar{I}_1}{3}}\right)^6 + \frac{42039}{67375n^4}\left(\sqrt{\frac{\bar{I}_1}{3}}\right)^8\right] \mathrm{dev}\left(\bar{\mathbf{B}}\right) \\
&= \frac{Nk_B\theta_0}{J}\left[1 + \frac{1}{5n}\bar{I}_1 + \frac{11}{175n^2}\bar{I}_1^2 + \frac{19}{875n^3}\bar{I}_1^3 + \frac{519}{67375n^4}\bar{I}_1^4\right] \mathrm{dev}\left(\bar{\mathbf{B}}\right),
\end{aligned}
\tag{26}
$$

which is equivalent to the expression obtained from deriving the expression from Arruda and Boyce [1993].

1.3 The Three-Chain Hyperelastic Model

The Three-Chain (TC or 3-ch) model from Wang and Guth [1952] consists in a network of three orthogonal non-Gaussian chains which deform affinely with the imposed bulk deformation [Arruda, 1992]. This model is an extension of the Treloar [1946] TC model with the consideration of Langevin chain statistics in the network [Arruda and Boyce, 1993].

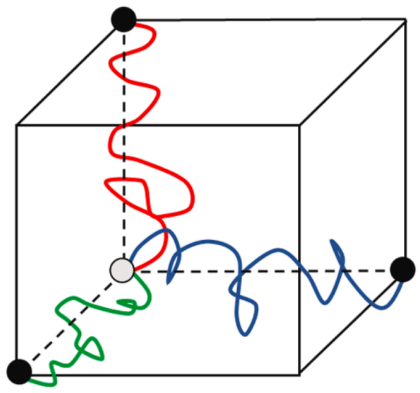

Fig. 4: Three-Chain model representation of the unit cell rubber network

In this model, the chains are located along the axes of the initially cubic cell. The chains deform affinely with the cell and the stretch on each chain will then correspond to a principal stretch

value. The resulting strain energy function writes [Boyce and Arruda, 2000]

$$\psi\left(\bar{\lambda}^*, J, \theta_0\right) = \frac{N k_B \theta_0 n}{3}\left[\frac{\lambda_1}{\sqrt{n}}\mathcal{L}^{-1}\left[\frac{\lambda_1}{\sqrt{n}}\right] + \ln\left(\frac{\mathcal{L}^{-1}\left[\frac{\lambda_1}{\sqrt{n}}\right]}{\sinh\,\mathcal{L}^{-1}\left[\frac{\lambda_1}{\sqrt{n}}\right]}\right)\right.$$
$$+ \frac{\lambda_2}{\sqrt{n}}\mathcal{L}^{-1}\left[\frac{\lambda_2}{\sqrt{n}}\right] + \ln\left(\frac{\mathcal{L}^{-1}\left[\frac{\lambda_2}{\sqrt{n}}\right]}{\sinh\,\mathcal{L}^{-1}\left[\frac{\lambda_2}{\sqrt{n}}\right]}\right)$$
$$\left. + \frac{\lambda_3}{\sqrt{n}}\mathcal{L}^{-1}\left[\frac{\lambda_3}{\sqrt{n}}\right] + \ln\left(\frac{\mathcal{L}^{-1}\left[\frac{\lambda_3}{\sqrt{n}}\right]}{\sinh\,\mathcal{L}^{-1}\left[\frac{\lambda_3}{\sqrt{n}}\right]}\right)\right] + \frac{k_0}{2}\left(J-1\right)^2. \tag{27}$$

$$\sigma_i = \frac{N k_B \theta_0}{3} \tag{28}$$

to be continued...

2 Finite Strain Viscoelastic Material Models

ajouter modèle Gen. Maxwell linéaire?

2.1 General Framework for Finite Strain Viscoelastic Deformations

The total deformation gradient $\mathbf{F}$ can be multiplicatively decomposed into elastic and viscous components as [Lee, 1969]

$$\mathbf{F} = \mathbf{F}^e\mathbf{F}^v, \tag{29}$$

where superscripts e and v stands for elastic and viscous.

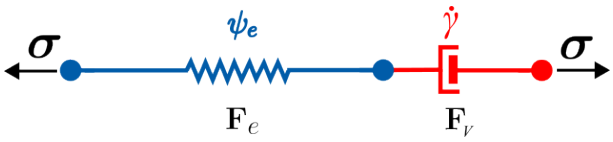

Fig. 5: Rheological representation of a single Maxwell element.

The theory from Boyce et al. [1988] starts with the additive decomposition of the velocity gradient $\mathbf{L}$, which can be expressed using the total deformation gradient $\mathbf{F}$ is related and the rate of total deformation gradient $\dot{\mathbf{F}}$ as

$$\mathbf{L} = \dot{\mathbf{F}}\mathbf{F}^{-1} = \dot{\mathbf{F}}^e\left(\mathbf{F}^e\right)^{-1} + \mathbf{F}^e\left[\dot{\mathbf{F}}^v\left(\mathbf{F}^v\right)^{-1}\right]\left(\mathbf{F}^e\right)^{-1} = \mathbf{L}^e + \mathbf{F}^e\mathbf{L}^v\left(\mathbf{F}^e\right)^{-1} = \mathbf{L}^e + \tilde{\mathbf{L}}^v. \tag{30}$$

The viscous velocity gradient $\mathbf{L}^v$ can be further split into symmetric and skew parts, as

$$\tilde{\mathbf{L}}^v = \mathbf{F}^e\mathbf{L}^v\left(\mathbf{F}^e\right)^{-1} = \tilde{\mathbf{D}}^v + \tilde{\mathbf{W}}^v, \tag{31}$$

where $\tilde{\mathbf{D}}^v$ is the viscous rate of deformation and $\tilde{\mathbf{W}}^v$ is the viscous spin tensor. The unloading process relating the deformed state with the intermediate state is not uniquely defined since an arbitrary rigid body rotation of the intermediate state leaves the state stress-free [Bergström, 2015]. The intermediate state can be made unique in different ways [Boyce et al., 1989]. Assuming the intermediate configuration is invariant to rigid body rotation, the skew part of the viscous velocity gradient is null $\tilde{\mathbf{W}}^v = \mathbf{0}$ [Bergström and Boyce, 1998]. In general, these assumptions will result in both inelastic and elastic deformation gradient containing rotations [Bergström, 2015]. The rate of viscous deformation is constitutively prescribed by defining the symmetric part of the viscous velocity gradient

$$\tilde{\mathbf{D}}^v = \dot{\gamma}\mathbf{N}, \tag{32}$$

where $\mathbf{N}$ is the tensor which provides the direction of the viscoelastic flow and $\dot{\gamma}$ is the effective deviatoric flow rate. Noting that $\boldsymbol{\sigma}$ is computed in the current configuration, the driving deviatoric stress in the relaxed configuration convected to the current configuration is its deviatoric part. Further defining the effective stress τ using the Frobenius norm, the direction of the

driving deviatoric stress writes

$$\mathbf{N} = \frac{\mathrm{dev}(\boldsymbol{\sigma})}{\tau} = \frac{\mathrm{dev}(\boldsymbol{\sigma})}{\sqrt{\mathrm{dev}(\boldsymbol{\sigma}) : \mathrm{dev}(\boldsymbol{\sigma})}} = \frac{\mathrm{dev}(\boldsymbol{\sigma})}{\sqrt{\mathrm{tr}\left[\mathrm{dev}(\boldsymbol{\sigma})\mathrm{dev}(\boldsymbol{\sigma})\right]}} \tag{33}$$

Hence, the time derivative of the viscous deformation gradient writes

$$\dot{\mathbf{F}}^v = \dot{\gamma} \left(\mathbf{F}^e\right)^{-1} \frac{\mathrm{dev}(\boldsymbol{\sigma})}{\tau} \mathbf{F} = \dot{\gamma} \mathbf{N} \mathbf{F}^v \tag{34}$$

The rate of viscous deformation equation is pivotal since it allows computing the evolution of the viscous strain $\mathbf{F}^v$ over time and, hence, compute the elastic part of the strain. A first approach to compute the viscous strain is to use an explicit scheme [Gilabert, 2021]

$$\mathbf{F}^v\left(t + \Delta t\right) = \mathbf{F}^v\left(t\right) + \Delta t \; \dot{\mathbf{F}}^v\left(t\right), \tag{35}$$

where t is the current time and Δt is the time increment. Using this approach, the time increment must however fulfill the Courant-Friedrichs-Lewy condition [Courant et al., 1967], which states that the time increment Δt must be typically smaller than the element size divided by the dilatational wave speed. Alternatively, a linearly implicit Euler scheme can be used

$$\mathbf{F}^v\left(t + \Delta t\right) = \mathbf{F}^v\left(t\right) + \Delta t \; \dot{\mathbf{F}}^v\left(t + \Delta t\right). \tag{36}$$

Due to the highly nonlinear nature of $\mathbf{F}^v$, the solution relies on the linearization process leading to the calculation of the Jacobian of $\dot{\mathbf{F}}^v$. The solution writes

$$\mathbf{F}^v\left(t + \Delta t\right) = \mathbf{F}^v\left(t\right) + \mathbb{H} : \dot{\mathbf{F}}^v\left(t\right), \text{ with } \mathbb{H} = \left(\frac{1}{\Delta t}\mathbb{I} - \frac{\partial \dot{\mathbf{F}}^v(t)}{\partial \mathbf{F}^v}\right)^{-1}, \tag{37}$$

where $\mathbb{H}$ is a fourth-order tensor containing the Jacobian $(\partial \dot{\mathbf{F}}^v / \partial \mathbf{F}^v)$ and $\mathbb{I}$ is the fourth-order identity tensor and ':' is the product of a fourth-order tensor with a second-order tensor, which writes $\mathbb{H} : \dot{\mathbf{F}} = H_{ijkl}\dot{F}_{kl}$ using index notation. The implicit scheme allows increasing the time increments above Courant condition, especially when coupled with a Newton-Raphson algorithm. Nonetheless, the construction of the Jacobian is not always analytically possible [Gilabert, 2021]. Finally, the elastic stress $\boldsymbol{\sigma}^e$ can be computed using the updated elastic deformation gradient given by

$$\mathbf{F}^e = \mathbf{F}\left(\mathbf{F}^v\right)^{-1}. \tag{38}$$

2.1.1 Evolution of viscous deformations using exponential mapping

Considering the initial value problem defined by the tensor ordinary differential equation

$$\dot{\mathbf{Y}}(t) = \mathbf{A}\mathbf{Y}(t), \tag{39}$$

with the initial condition

$$\mathbf{Y}(t_0) = \mathbf{Y}_0, \tag{40}$$

where $\mathbf{A}$ and $\mathbf{Y}_0$ are given constant tensors (generally unsymmetric). The *tensor exponential map* $\exp[\cdot]$ is the unique solution to the above problem [de Souza Neto et al., 2008; Weber and Anand, 1990]

$$\mathbf{Y}(t) = \exp\left[(t - t_0)\mathbf{A}\right]\mathbf{Y}_0. \tag{41}$$

By letting $\mathbf{A}$ be a function of time t, the exact solution provided in Equation (41) can be used to generate approximated solutions de Souza Neto et al. [2008]. Similarly to the generalized midpoint algorithm based on standard Euler approximation, it is possible to approximate the solution by a similar algorithm based on the exponential map, the *generalized exponential map midpoint rule*. The algorithm approximates $\mathbf{Y}_{n+1}$ as the exact solution that would be obtained at t_{n+1} if $\mathbf{A}$ was constant over the time interval $[t_n,\ t_{n+1}]$. The update formula yields [de Souza Neto et al., 2008]

$$\mathbf{Y}_{n+1} = \exp\left[\Delta t\mathbf{A}\left(t_{n+\theta}\right)\right]\mathbf{Y}_n, \tag{42}$$

where $\Delta t = t_{n+1} - t_n$ and $t_{n+\theta} = t_n + \theta\Delta t$, with prescribed parameter $0 \leq \theta \leq 1$.

The *explicit* exponential map integrator is obtained when $\theta = 0$, whilst the *backward* (or fully *implicit*) exponential map integrator is obtained when $\theta = 1$. When $\theta = \frac{1}{2}$ the *midpoint* exponential map integrator is obtained, which is the only second-order accurate integrator (first-order otherwise) [de Souza Neto et al., 2008].
Applied to the viscous deformation gradient with Equation (34), the *explicit* update formula writes

$$\mathbf{F}^v_{n+1} = \exp\left[\Delta t\dot{\gamma}_n\mathbf{N}_n\right]\mathbf{F}^v_n, \tag{43}$$

which can be computed with the quantities from previous time step. On the other hand, the *implicit* update formula

$$\mathbf{F}^v_{n+1} = \exp\left[\Delta t\dot{\gamma}_{n+1}\mathbf{N}_{n+1}\right]\mathbf{F}^v_n \tag{44}$$

need to be solved by an iterative procedure. A local Newton-Raphson iteration scheme can be employed at each integration point within the domain of a finite element based on the reformulation of Equation (44) as a residual expression [Platen et al., 2024]

$$\mathbf{R} = \mathbf{F}^v_{n+1} - \exp\left[\Delta t\dot{\gamma}_{n+1}\mathbf{N}_{n+1}\right]\mathbf{F}^v_n \tag{45}$$

Algorithm 1 Implicit update of the viscous deformation gradient

Require: $\mathbf{F}_n,\ \mathbf{F}_n^v$ ▷ from **GP0**

Require: $\mathbf{F}_{n+1},\ \Delta t = t_{n+1} - t_n$ ▷ from **GP1**

$\mathbf{F}_{n+1}^v \leftarrow \mathbf{F}_n^v$ ▷ Elastic trial

while $i <$ ITMAX **do** ▷ Newton-Raphson

Compute $\boldsymbol{\sigma}_{n+1},\ p_{n+1}$

$\mathbf{N} \leftarrow \frac{\mathrm{dev}(\boldsymbol{\sigma}_{n+1})}{||\mathrm{dev}(\boldsymbol{\sigma}_{n+1})||}$ ▷ Direction of flow

$\dot{\gamma} \leftarrow f\left(\boldsymbol{\sigma}_{n+1},\ p_{n+1}\right)$ ▷ Creep factor

$\mathbf{R} \leftarrow \mathbf{F}_{n+1}^v - \exp\left[\Delta t \dot{\gamma} \mathbf{N}\right] \cdot \mathbf{F}_n^v$ ▷ Residual

if $||\mathbf{R}|| \leq$ TOL **then**

GP1 $\leftarrow \mathbf{F}_{n+1}^v$

break

end if

$\mathbb{K} \leftarrow \frac{\partial \mathbf{R}}{\partial \mathbf{F}_{n+1}^v}$ ▷ Inelastic corrector

$\mathbf{F}_{n+1}^v \leftarrow \mathbf{F}_{n+1}^v - \mathbb{K}^{-1} : \mathbf{R}$

$i \leftarrow i + 1$

end while

To further reduce the number of operations within the Newton-Raphson procedure, the implicit update formula Equation (44) can be re-written as

$$\mathbf{F}_{n+1}^v = \exp\left[\Delta t \dot{\gamma}_{n+1} (\mathbf{F}_{n+1}^e)^{-1} \mathbf{N}_{n+1} \mathbf{F}_{n+1}^e\right] \mathbf{F}_n^v = (\mathbf{F}_{n+1}^e)^{-1} \exp\left[\Delta t \dot{\gamma}_{n+1} \mathbf{N}_{n+1}\right] \mathbf{F}_{n+1}^e \mathbf{F}_n^v, \tag{46}$$

so that the following equality is obtained

$$\mathbf{F} (\mathbf{F}_n^v)^{-1} = \exp\left[\Delta t \dot{\gamma}_{n+1} \mathbf{N}_{n+1}\right] \mathbf{F}_{n+1}^e. \tag{47}$$

The quantity $\mathbf{F}(\mathbf{F}_n^v)^{-1} = \mathbf{F}_{trial}^e$ actually corresponds to the elastic deformation gradient if the current step is fully elastic. Using the inverse property of the exponential map integrator [Korelc and Stupkiewicz, 2014]

$$\mathbf{F}_{n+1}^e = \exp\left[-\Delta t \dot{\gamma}_{n+1} \mathbf{N}_{n+1}\right] \mathbf{F}_{trial}^e, \tag{48}$$

allows rewriting the residual expression as

$$\mathbf{R} = \mathbf{F}_{n+1}^e - \exp\left[-\Delta t \dot{\gamma}_{n+1} \mathbf{N}_{n+1}\right] \mathbf{F}_{trial}^e. \tag{49}$$

Algorithm 2 Implicit update of the viscous deformation gradient using $\mathbf{F}^e$

Require: $\mathbf{F}_n,\ \mathbf{F}_n^v$ ▷ from **GP0**

Require: $\mathbf{F}_{n+1},\ \Delta t = t_{n+1} - t_n$ ▷ from **GP1**

$\mathbf{F}^e_{trial} \leftarrow \mathbf{F}_{n+1}(\mathbf{F}_n^v)^{-1}$ ▷ Elastic trial

$\mathbf{F}^e_{n+1} \leftarrow \mathbf{F}^e_{trial}$

while $i <$ ITMAX **do** ▷ Newton-Raphson

  Compute $\boldsymbol{\sigma}_{n+1},\ p_{n+1}$

  $\mathbf{N} \leftarrow \frac{\mathrm{dev}(\boldsymbol{\sigma}_{n+1})}{||\mathrm{dev}(\boldsymbol{\sigma}_{n+1})||}$ ▷ Direction of flow

  $\dot{\gamma} \leftarrow f\left(\boldsymbol{\sigma}_{n+1},\ p_{n+1}\right)$ ▷ Creep factor

  $\mathbf{R} \leftarrow \mathbf{F}^e_{n+1} - \exp\left[-\Delta t \dot{\gamma} \mathbf{N}\right] \cdot \mathbf{F}^e_{trial}$ ▷ Residual

  if $||\mathbf{R}|| \leq$ TOL **then**

    $\mathbf{F}^v_{n+1} \leftarrow \exp\left[\Delta t \dot{\gamma} \mathbf{N}\right] \cdot \mathbf{F}^v_n$

    GP1 $\leftarrow \mathbf{F}^v_{n+1}$

    break

  end if

  $\mathbb{K} \leftarrow \frac{\partial \mathbf{R}}{\partial \mathbf{F}^e_{n+1}}$ ▷ Elastic corrector

  $\mathbf{F}^e_{n+1} \leftarrow \mathbf{F}^e_{n+1} - \mathbb{K}^{-1} : \mathbf{R}$

  $i \leftarrow i + 1$

end while

2.1.2 Connection with other finite strain viscoelastic models

With approach from Boyce et al. [1988], this model replicates the model that has been developed by Reese and Govindjee [1998] when a "constant" deformation rate is applied [Reese and Govindjee, 1998; Dal and Kaliske, 2009]. Note that "constant" in this case refers to the deformation rate not depending on the strain and/or stress levels, where it can still depend on other parameters such as temperature. The update equation from Reese and Govindjee [1998] writes

$$\dot{\mathbf{C}}^v = \frac{1}{\eta} \left(\mathbf{F}^v\right)^T \left(\mathbf{F}^e\right)^{-1} \mathrm{dev}\left(\boldsymbol{\sigma}\right) \mathbf{F}^e \mathbf{F}^v, \tag{50}$$

where η is the viscosity. The right Cauchy-Green tensor rate $\dot{\mathbf{C}}$ can be linked to the rate of deformation as [Gouhier and Diani, 2024]

$$\dot{\mathbf{C}} = 2\mathbf{F}^T \mathbf{D} \mathbf{F}. \tag{51}$$

Using the relations from Equations (31) to (33), Equation (51) allows writing

$$\begin{aligned}\dot{\mathbf{C}}^v &= 2\left(\mathbf{F}^v\right)^T \mathbf{D}^v \mathbf{F}^v \\ &= 2\left(\mathbf{F}^v\right)^T \left(\mathbf{F}^e\right)^{-1} \tilde{\mathbf{D}}^v \mathbf{F}^e \mathbf{F}^v \\ &= 2\left(\mathbf{F}^v\right)^T \left(\mathbf{F}^e\right)^{-1} \dot{\gamma} \mathbf{N} \mathbf{F}^e \mathbf{F}^v \\ &= 2\left(\mathbf{F}^v\right)^T \left(\mathbf{F}^e\right)^{-1} \dot{\gamma} \frac{\mathrm{dev}(\boldsymbol{\sigma})}{\tau} \mathbf{F}^e \mathbf{F}^v,\end{aligned} \tag{52}$$

and from there, the update relation from Reese and Govindjee [1998] is recovered for

$$\dot{\gamma} = \frac{\tau}{2\eta}. \tag{53}$$

2.2 The Three Network Material Model

The Three Network (TN) model was originally developed for mechanical behavior prediction of thermoplastic materials [Bergström, 2015]. The total deformation gradient $\mathbf{F}$ is decomposed into a mechanical part $\mathbf{F}^m$ and a thermal part $\mathbf{F}^{th}$ which is related to thermal expansion (in this case isotropic).

$$\mathbf{F} = \mathbf{F}^m \mathbf{F}^{th} = \mathbf{F}^m \left[1 + \alpha(\theta - \theta_0)\right] \mathbf{I}, \tag{54}$$

where α is the isotropic thermal expansion coefficient.

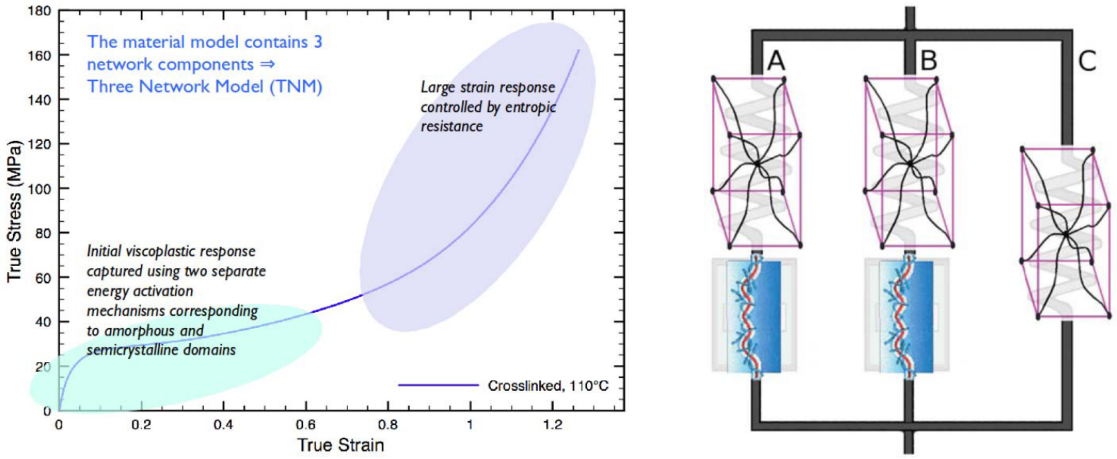

(a) **(b)**

Fig. 6: Separation of the stress-strain curve into the different deformation mechanisms for the TN model (a) and rheological representation of the TN model (b) [Bergström and Bischoff, 2010].

The kinematics of the TN model consists of 3 molecular networks (A, B and C) acting in parallel as shown in the rheological representation Fig. 6b, which yields

$$\mathbf{F}^m = \mathbf{F}^m_A = \mathbf{F}^m_B = \mathbf{F}^m_C \tag{55}$$

$$\boldsymbol{\sigma} = \boldsymbol{\sigma}_A + \boldsymbol{\sigma}_B + \boldsymbol{\sigma}_C \tag{56}$$

In this model, the initial viscoplastic response is controlled using two separate energy activation mechanisms (network A and B) which actually correspond to the amorphous and semicrystalline domains. The large strain response is controlled by entropic resistance (network C). This decomposition of the response can be observed in Fig. 6a

The total (mechanical) deformation gradient acting on network A is multiplicatively decomposed into a viscous $\mathbf{F}^v_A$ and an elastic $\mathbf{F}^e_A$

$$\mathbf{F}^m_A = \mathbf{F}^e_A \mathbf{F}^v_A. \tag{57}$$

The Cauchy stress acting on network A is given by the EC model with the addition of a temperature-dependence term

$$\boldsymbol{\sigma}_A = \frac{\mu_A}{J^e_A \bar{\lambda}^{e*}_A} \left[1 + \frac{\theta - \theta_0}{\hat{\theta}}\right] \frac{\mathcal{L}^{-1}\left(\frac{\bar{\lambda}^{e*}_A}{\lambda^{lock}}\right)}{\mathcal{L}^{-1}\left(\frac{1}{\lambda^{lock}}\right)} \operatorname{dev}\left(\bar{\mathbf{B}}^{\mathbf{e}}_{\mathbf{A}}\right) + k_0 \left(J^e_A - 1\right) \mathbf{I} \tag{58}$$

where $\hat{\theta}$ is a material parameter accounting for the temperature response of the stiffness. The effective deviatoric flow rate is given by the reptation-inspired equation [Bergström and Boyce, 2000]

$$\dot{\gamma}_A = \dot{\gamma}_0 \left(\frac{\tau_A}{\hat{\tau}_A + aR(p_A)} \right)^{m_A} \left(\frac{\theta}{\theta_0} \right)^n \tag{59}$$

where $\dot{\gamma}_0$ [s^{-1}] is the initial effective flow rate, p_a is the hydrostatic pressure, $R(x) = (x + |x|)/2$ is the ramp function, $\hat{\tau}_A$ is the flow resistance, a is the pressure dependence of the flow, m_A is the stress exponential and n is the temperature exponential.

For network B, the reasoning is similar to network A. However, in this case, the effective shear modulus μ_B is taken to evolve with the effective deviatoric flow rate from an initial value μ_{Bi} as

$$\dot{\mu}_B = -\beta \left[\mu_B - \mu_{Bf} \right] \dot{\gamma}_A$$

where β is the evolution rate and μ_{Bf} is the final value of μ_B. This expression allows to better capture the distributed yielding that is observed for many thermoplastics [Bergström, 2015]. The definition of the viscous flow rule is equivalent to network A. For network C, there is no viscous contribution to the deformation tensor. Hence, the temperature-dependent EC model writes

$$\boldsymbol{\sigma}_C = \frac{\mu_A}{J^m \bar{\lambda}^*} \left[1 + \frac{\theta - \theta_0}{\hat{\theta}} \right] \frac{\mathcal{L}^{-1}\left(\frac{\bar{\lambda}^*}{\lambda^{lock}} \right)}{\mathcal{L}^{-1}\left(\frac{1}{\lambda^{lock}} \right)} \operatorname{dev}\left(\bar{\mathbf{B}} \right) + k_0 \left(J^m - 1 \right) \mathbf{I}. \tag{60}$$

For some materials such as ultra-high molecular weight polyethylene (UHMWPE), a first order I_2 dependence is added to network C as [Bergström and Bischoff, 2010]

$$\begin{aligned} \boldsymbol{\sigma}_C = & \frac{1}{1+q} \left\{ \frac{\mu_A}{J^m \bar{\lambda}^*} \left[1 + \frac{\theta - \theta_0}{\hat{\theta}} \right] \frac{\mathcal{L}^{-1}\left(\frac{\bar{\lambda}^*}{\lambda^{lock}} \right)}{\mathcal{L}^{-1}\left(\frac{1}{\lambda^{lock}} \right)} \operatorname{dev}\left(\bar{\mathbf{B}} \right) \right. \\ & \left. + q \frac{\mu_C}{J} \left[\bar{I}_1 \operatorname{dev}\left(\bar{\mathbf{B}} \right) - \frac{2}{3} \bar{I}_2 \mathbf{I} - \operatorname{dev}\left(\bar{\mathbf{B}} \right)^2 \right] + k_0 \left(J^m - 1 \right) \mathbf{I} \right\}., \end{aligned} \tag{61}$$

where q controls the I_2-dependence. The added terms in Eq. (61) actually correspond to the Mooney-Rivlin material model with $C_1 = 0$ and $C_2 = \mu_c/2$.

2.2.1 Example: calibration of a Three Network model for unfilled PEEK

In his book, Bergström [2015] conducts a study over a few material models for the modeling of unfilled Polyether Ether Ketone (PEEK). He showed that calibrating the TN model based on uniaxial compression/tension test gave the smallest error with respect to the other material models. This shows that the TN model has a great predictive capability for PEEK.

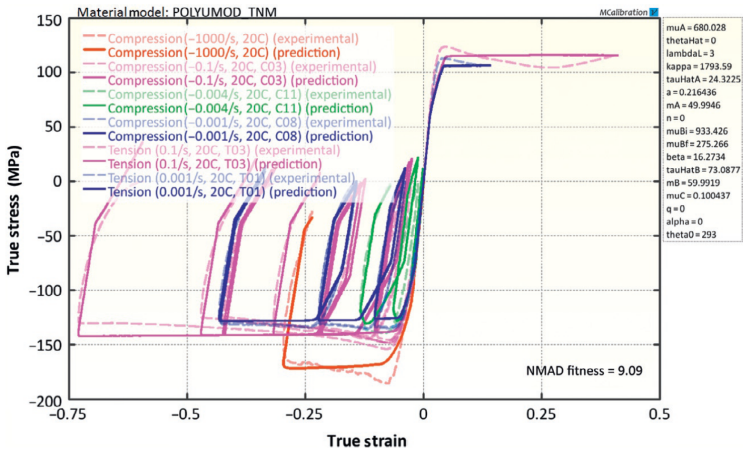

(a)

Material Model	Error in Model Calibration (%)
Elastic-plastic with isotropic hardening and rate-dependence	127
Arruda-Boyce eight-chain	68.4
Yeoh	59.6
DNF	30.9
Elastic-plastic with kinematic hardening and rate-dependent creep (three backstress)	30.6
Johnson-Cook	24.8
BB	24.4
Parallel Network model with two networks (Power flow, yield evolution, pressure dependence)	16.5
Parallel Network model with three networks (Power flow, yield evolution, pressure dependence)	9.1
Three Network model	9.1

(b)

Fig. 7: Calibration of the Three Network model from uniaxial compression/tension tests on unfilled PEEK (a) and comparison of the resulting error from calibration for other material models (b) [Bergström, 2015].

Bergström [2015] has then tested few of the calibrated material models by comparing data from an indentation testing (spherical indenter) with a Finite Element (FE) model. The results show that among the tested material models, the TN model gives the most satisfactory results even though the calibration was carried on uniaxial data and the indentation problem is multiaxial.

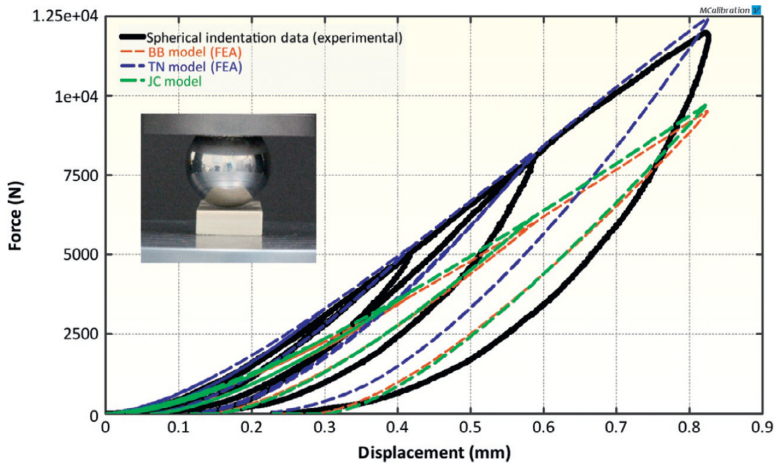

Fig. 8: Comparison of experimental and FE results from a small punch experiment using few material models calibrated using uniaxial compression/tension data [Bergström, 2015].

2.2.2 Example: calibration of a Three Network model for UHMWPE

In their work, Bergström and Bischoff [2010] have used the three-network material model for the modelling of ultra-high molecular weight polyethylene (UHMWPE). The particularity for this material is that the Three-Network model uses the I_2-dependence terms for better accuracy.

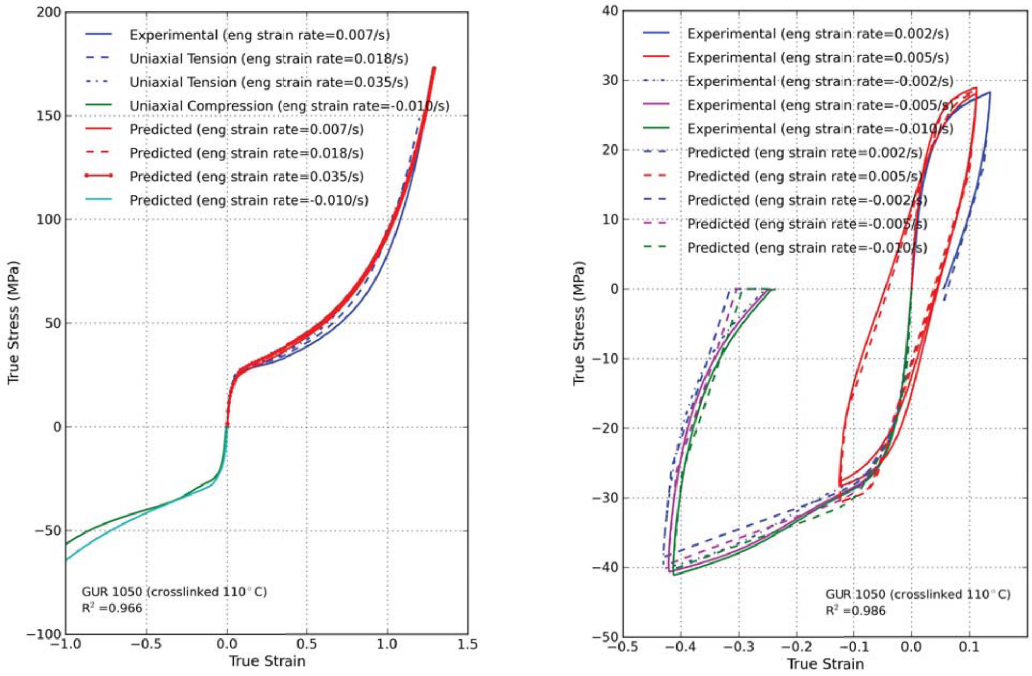

(a) **(b)**

Fig. 9: Calibration results of the Three Network model from uniaxial compression/tension tests on UHMWPE (a) and (b) [Bergström and Bischoff, 2010].

From the uniaxial model calibration results in Fig. 9, Bergström and Bischoff [2010] have obtained a set of optimal parameters which are gathered in Table 1.

Table 1: Material parameters for the TN model with UHMWPE [Bergström and Bischoff, 2010].

Symbol	Value	Description
μ_A	200 MPa	Shear modulus of network A
λ_L	3.25	Locking stretch
κ	6000 MPa	Bulk modulus
$\hat{\tau}_A$	3.25 MPa	Flow resistance of network A
a	0.073	Pressure dependence of flow
$m_A = m_b$	20	Stress exponential of network A
μ_{Bi}	293 MPa	Initial shear modulus of network B
μ_{Bf}	79.1 MPa	Final shear modulus of network B
β	31.9	Evolution rate of μ_B
$\hat{\tau}_B$	20.1 MPa	Flow resistance of network B
μ_C	10.0 MPa	Shear modulus of network C
q	0.23	Relative contribution of I_2 of network C

Using the calibrated material model, they have successfully reproduced the results from an experimental punch test in Fig. 10b using a 3D finite element model in Abaqus/Standard Fig. 10a.

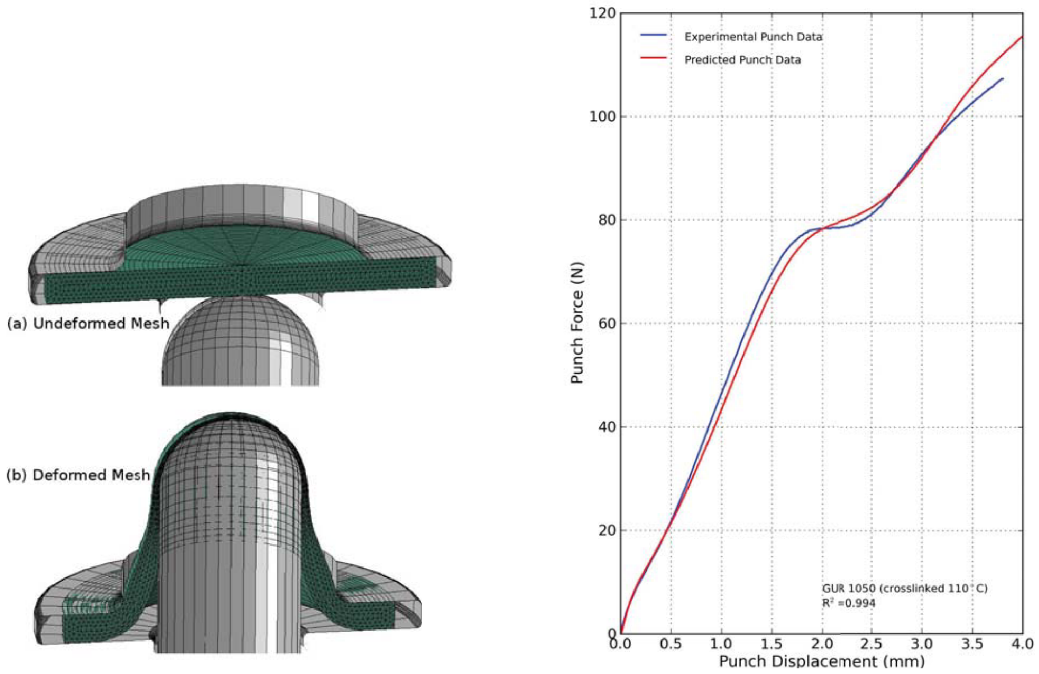

(a) **(b)**

Fig. 10: Finite element representation of the experimental punch test (a) and comparison between experimental data and finite element prediction for UHMWPE in small punch loading (b) [Bergström and Bischoff, 2010].

2.3 The Boyce-Parks-Argon Model

The Boyce-Parks-Argon (BPA) model was developed for glassy amorphous polymers. The stress-strain behavior of those polymers can be interpreted using both intermolecular and network resistances [Boyce et al., 1988]. The intermolecular resistance represents the barrier of deformation to overcome while the network resistance is an entropic resistance due to the polymer chain reorientation, showing the rubbery effect with a nonlinear stress increase.

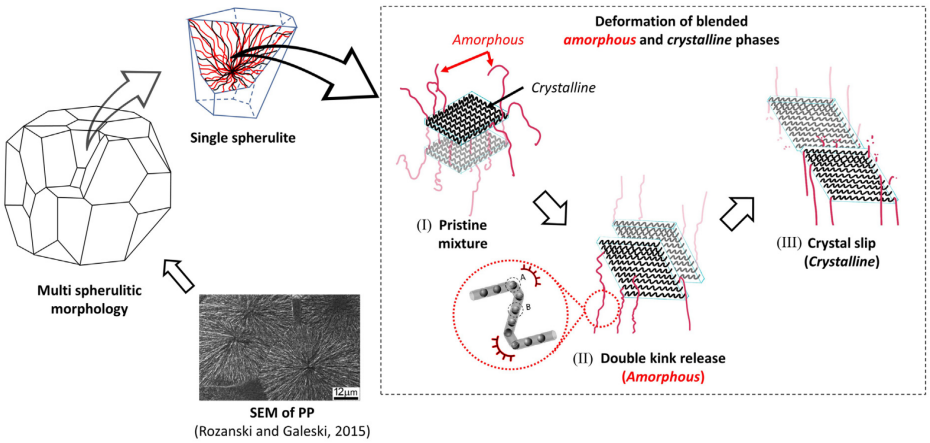

Fig. 11: Schematic description of yield kinetics for semi-crystalline polymers by as spherulite unit processing amorphous and crystalline phases [Hao et al., 2022a].

The intermolecular resistance was developed using the concept of 'double kink' release process

of the polymer chain to account for the thermally-activated yielding mechanism [Argon, 1973]. Rate-, temperature- and pressure-dependencies were prescribed in the flow rule by proposing an equivalent plastic strain as

$$\dot{\gamma}^p = \dot{\gamma}_0 \exp\left[-\frac{A(s+\alpha p)}{\theta}\left(1-\left[\frac{\tau}{s+\alpha p}\right]^{5/6}\right)\right], \tag{62}$$

where θ is the absolute temperature, $\dot{\gamma}_0$ and A are the rate-dependent sensitivity parameters that are identified from the peak yield stress at different strain rates, α is the pressure-dependent parameter and p is the hydrostatic pressure. The driving stress is given by the equivalent stress $\tau = \sqrt{(1/2)\text{dev}(\boldsymbol{\sigma}) : \text{dev}(\boldsymbol{\sigma})}$ and s is the so-called athermal strength. Argon [1973] original law was modified heuristically by Boyce et al. [1988] to incorporate the post-yield softening. Strength s represents the current athermal deformation resistance of the material indicating the current state of the structure. To avoid involving any specific testing technique, Boyce et al. [1988] adopted a phenomenological softening evolution equation to facilitate the model usage. Strain softening depends on plastic strain rate, temperature, and on the favorable saturated structure state as

$$\dot{s} = h\left(1-\frac{s}{s_1}\right)\dot{\gamma}^p, \tag{63}$$

where the material constant h is the softening slope from the peak yield stress to the saturated low stress and s_1 is the value of s when the saturated state is reached.

2.4 The Modified Boyce-Parks-Argon Model

The Boyce-Parks-Argon model was further modified by Chowdhury et al. [2008] to account for the pre-yield hardening, leading to the Modified Boyce-Parks-Argon (MBPA) model. The reformulation of $\dot{s}$ was later validated for epoxy resin by Poulain et al. [2014], assuming a von Mises-like stress. Hence, the driving stress is represented using the effective stress $\sigma_{eq} = \sqrt{3}\tau$ and the effective strain rate $\dot{\bar{\varepsilon}} = \dot{\gamma}^p/\sqrt{3}$, yielding

$$\tilde{\mathbf{D}}^v = \dot{\bar{\varepsilon}}\,\mathbf{N}, \text{ with } \mathbf{N} = \frac{3}{\sqrt{2}}\frac{\text{dev}\,(\boldsymbol{\sigma})}{\sigma_{eq}} \tag{64}$$

The concept of this modified model is to represent the observed nonlinear response before the peak yield by mirroring the post-yield softening to the pre-yield hardening [Hao et al., 2022a], leading to a new evolution law of the athermal strength s given by

$$\dot{s} = H_1\left(1-\frac{s}{s_1}\right)\dot{\bar{\varepsilon}} + H_2\left(1-\frac{s}{s_2}\right)\dot{\bar{\varepsilon}}, \tag{65}$$

where s_1 is the athermal strength related to peak yield and s_2 is related to the saturated stress. The initial value s_0 in the MBPA model correlated to the initiation of the nonlinearity. H_1 and H_2 are the smooth, Heaviside-like functions that respectively control the activation of hardening

or softening depending on current strain level, as

$$H_1 = -h_1 \left[\tanh\left(\frac{\bar{\varepsilon} - \bar{\varepsilon}_p}{f\bar{\varepsilon}_p} \right) - 1 \right]; \tag{66}$$

$$H_2 = h_2 \left[\tanh\left(\frac{\bar{\varepsilon} - \bar{\varepsilon}_p}{f\bar{\varepsilon}_p} \right) + 1 \right], \tag{67}$$

where $\bar{\varepsilon}_p$ is the plastic strain at peak yield, and h_1 and h_2 are the hardening and softening slopes, respectively.

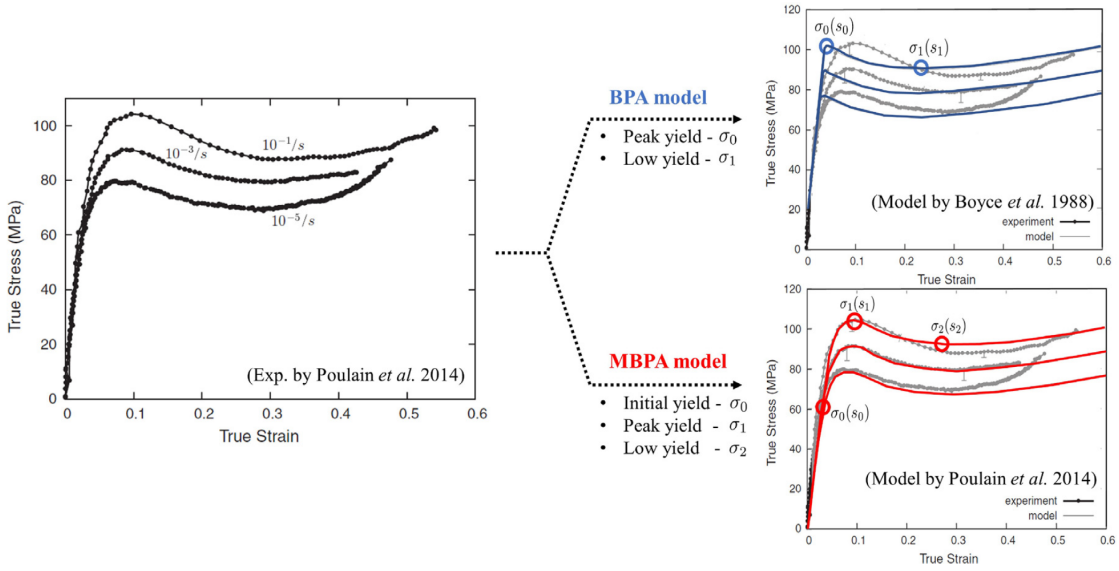

Fig. 12: Different strain softening evolution laws of the thermal strength s for epoxy resin using the BPA and MBPA model [Hao et al., 2022a].

2.5 The Unified Semi-Crystalline Polymer Model

The Unified Semi-Crystalline Polymer (USCP) model is a generalization of the MBPA [Hao et al., 2023] with the addition of a single viscoplastic law that unifies both amorphous and crystalline phases of the polymer. The USCP model was initially developed for thermoplastic polymers but can also be used to model the response of thermoset polymers (e.g. epoxy resin) by deactivation the crystalline phase. The later model actually corresponds to the MBPA model, which has been initially developed by Poulain et al. [2014].

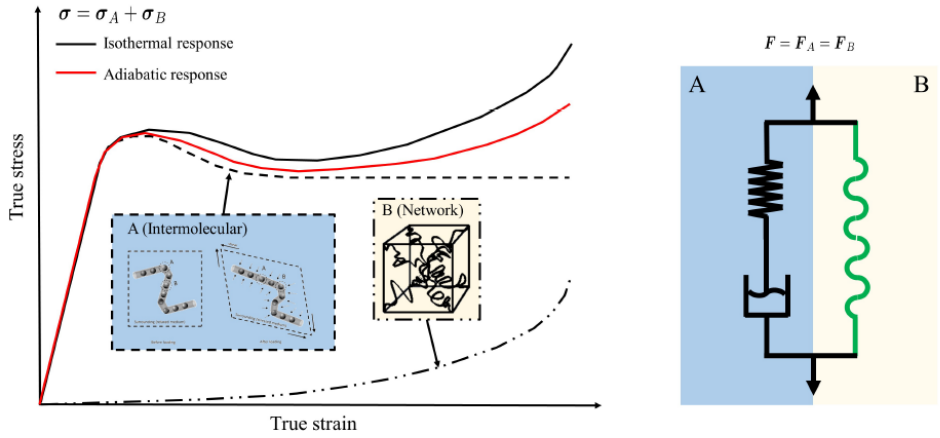

Fig. 13: Schematic stress-strain representation of intermolecular -A- and network -B- resistances (left) and the corresponding rheological model (right) [Hao et al., 2023].

Intermolecular (A) and network (B) resistances share the same deformation gradient in the assumed parallel arrangement

$$\mathbf{F} = \mathbf{F}_A = \mathbf{F}_B, \tag{68}$$

hence leading to the total Cauchy stress

$$\boldsymbol{\sigma} = \boldsymbol{\sigma}_A + \boldsymbol{\sigma}_B. \tag{69}$$

For branch A, the deformation gradient $\mathbf{F}$ is decomposed into an elastic and plastic components as

$$\mathbf{F} = \mathbf{F}_A^e \mathbf{F}_A^p, \tag{70}$$

and the rate of viscous deformation is obtained as defined in the MBPA model, hence

$$\dot{\mathbf{F}}_A^p = \dot{\bar{\varepsilon}}\, \mathbf{N}_A \mathbf{F}_A^p. \tag{71}$$

The effective plastic strain rate $\dot{\bar{\varepsilon}}$ is obtained from the thermally-activated double kink theory with free energy barrier [Hao et al., 2023], which is similar to the BPA model, as

$$\dot{\bar{\varepsilon}} = \dot{\varepsilon}_0 \exp\left[-\frac{A(s+\alpha p)}{\theta}\left(1 - \left[\frac{\sigma_{eq}}{s+\alpha p}\right]^m\right)\right], \tag{72}$$

where θ is the absolute temperature and p is the hydrostatic pressure. Material constants $\dot{\varepsilon}_0$, m, A are rate-dependent sensitivity parameters that can be identified through parameter identification using the peak yield stress at minimum two strain rate values [Hao et al., 2023]. The magnitude s is the so-called athermal effective stress and α is the pressure sensitivity parameter useful to capture tension-compression asymmetry. The driving stress is defined as the equivalent stress τ. The temperature-dependent elastic modulus $E(\theta)$ is assumed to follow

a logarithmic evolution form between current and reference temperature as

$$E(\theta) = \frac{E_{ref}}{10^{\beta(\theta-\theta_{ref})}},\ G(\theta) = \frac{E(\theta)}{2(1+\nu)} \tag{73}$$

where β is a material parameter and the subscript $_{ref}$ denotes the reference value. $G(\theta)$ is the temperature-dependent shear modulus and ν is the Poisson coefficient. The initial athermal effective stress value s_0 writes [Poulain et al., 2014]

$$s_0 = \sqrt{3}\frac{8.5^{-1/m}}{1-\nu}\frac{E(\theta)}{2(1+\nu)} = \sqrt{3}\frac{8.5^{-1/m}}{1-\nu}G(\theta). \tag{74}$$

The evolution law for the athermal effective stress is formulated using a smooth Heaviside-like function to characterize pre-peek hardening (H_1), post-peak softening (H_2) and second yield (H_3) due to the crystalline phase contribution as

$$\dot{s} = H_1(\bar{\varepsilon})\left(1-\frac{s}{s_1}\right)\dot{\bar{\varepsilon}} + H_2(\bar{\varepsilon})\left(1-\frac{s}{s_2}\right)\dot{\bar{\varepsilon}} + H_3(\bar{\varepsilon})\left(1-\frac{s}{s_3}\right)\dot{\bar{\varepsilon}}, \tag{75}$$

where athermal strengths s_1, s_2 and s_3 correspond to the preferred state at different stages [Hao et al., 2022a]. The Heaviside functions involve three hardening/softening parameters h_1, h_2 and h_3, a smoothing factor f, plastic strain at peak yielding point $\bar{\varepsilon}_p$ and characteristic plastic strain $\bar{\varepsilon}_c$ when the crystalline nano-blocks initiates to yield [Hao et al., 2022a], and write

$$H_1(\bar{\varepsilon}) = -h_1\left[\tanh\left(\frac{\bar{\varepsilon}-\bar{\varepsilon}_p}{f\bar{\varepsilon}_p}\right)-1\right], \tag{76}$$

$$H_2(\bar{\varepsilon}) = h_2\left[1-\tanh\left(\frac{\bar{\varepsilon}-\bar{\varepsilon}_p}{f\bar{\varepsilon}_p}\right)\tanh\left(\frac{\bar{\varepsilon}-\bar{\varepsilon}_c}{f\bar{\varepsilon}_c}\right)\right], \tag{77}$$

$$H_3(\bar{\varepsilon}) = h_3\left[\tanh\left(\frac{\bar{\varepsilon}-\bar{\varepsilon}_c}{f\bar{\varepsilon}_c}\right)+1\right]. \tag{78}$$

When dealing with glassy amorphous polymers, the crystalline phase-related parameters are neglected, leading to the MBPA model from Poulain et al. [2014].

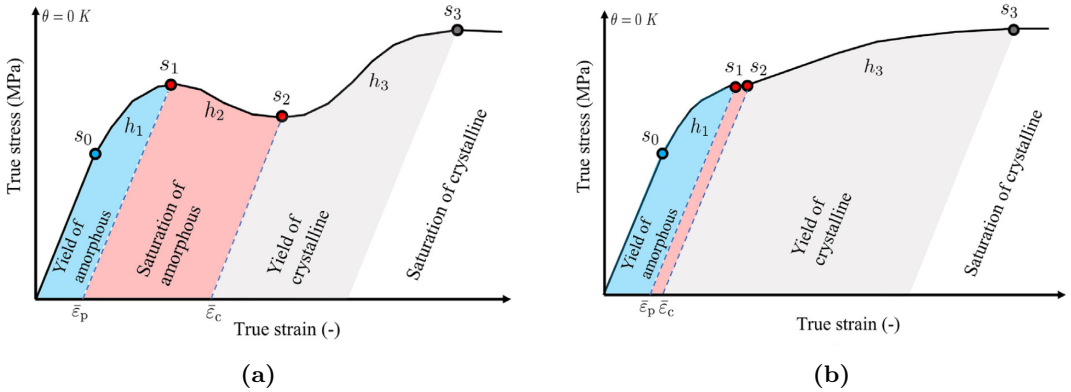

Fig. 14: Two representative types of true stress-strain curves with the proposed athermal strengths at absolute temperature 0K [Hao et al., 2022a].

The elastic stress contribution from branch A is computed from the updated elastic deformation

gradient $\mathbf{F}_A^e$, which is obtained from

$$\mathbf{F}_A^e = \mathbf{F}\left(\mathbf{F}_A^p\right)^{-1}, \tag{79}$$

and is represented by the most basic linear elastic element [Hao et al., 2022a], i.e. the Saint-Venant hyperelastic potential. The Saint-Venant hyperelastic potential leads to the following Pk2 stress tensor

$$\mathbf{S} = \lambda \mathrm{tr}\left(\mathbf{E}^{GL}\right)\mathbf{I} + 2\mu\mathbf{E}^{GL}, \tag{80}$$

where λ and μ are the Lamé parameters, and $\mathbf{E}^{GL}$ is the Green-Lagrange strain tensor. Let us recall that

$$\mathbf{E}^{GL} = \frac{1}{2}\left(\mathbf{U}^2 - \mathbf{I}\right), \tag{81}$$

$$\mathbf{U}^2 = \mathbf{F}^T\mathbf{F} = \mathbf{C}, \tag{82}$$

$$\boldsymbol{\sigma} = \frac{1}{J}\mathbf{F}\mathbf{S}\mathbf{F}^T, \tag{83}$$

where $\mathbf{C}$ is the left Cauchy-Green strain tensor and $J = \det\mathbf{C}$. The Pk2 stress tensor may be written as

$$\mathbf{S} = \lambda \mathrm{tr}\left(\frac{1}{2}\left[\mathbf{C} - \mathbf{I}\right]\right)\mathbf{I} + 2\mu\frac{1}{2}\left(\mathbf{C} - \mathbf{I}\right) = \frac{\lambda}{2}\left(\mathrm{tr}\mathbf{C} - 3\right)\mathbf{I} + \mu\left(\mathbf{C} - \mathbf{I}\right) = \left[\frac{\lambda}{2}\left(\mathrm{tr}\mathbf{C} - 3\right) + \mu\right]\mathbf{I} + \mu\mathbf{C} \tag{84}$$

and, consequently, the Cauchy stress tensor writes

$$\boldsymbol{\sigma} = \frac{1}{J}\left[\frac{\lambda}{2}\left(\mathrm{tr}\mathbf{C} - 3\right) + \mu\right]\mathbf{B} + \frac{1}{J}\mu\mathbf{B}^2. \tag{85}$$

For the branch B, the stress contribution $\boldsymbol{\sigma}_B$ is obtained from the combination of the three- and eight-chains models as [Wu and van der Giessen, 1993]

$$\boldsymbol{\sigma}_B = (1-\kappa)\boldsymbol{\sigma}_B^{3-ch} + \kappa\boldsymbol{\sigma}_B^{8-ch}, \tag{86}$$

where κ is a weight factor defined from the maximum principal stretch value λ_{max} as

$$\kappa = 0.85\frac{\lambda_{max}}{\sqrt{n}}. \tag{87}$$

2.5.1 Model identification under isothermal conditions

A material parameter identification procedure has been developed in Hao et al. [2022b]. This procedure requires a minimum of two true stress-strain curves at low strain rates, and proceeds following three steps.

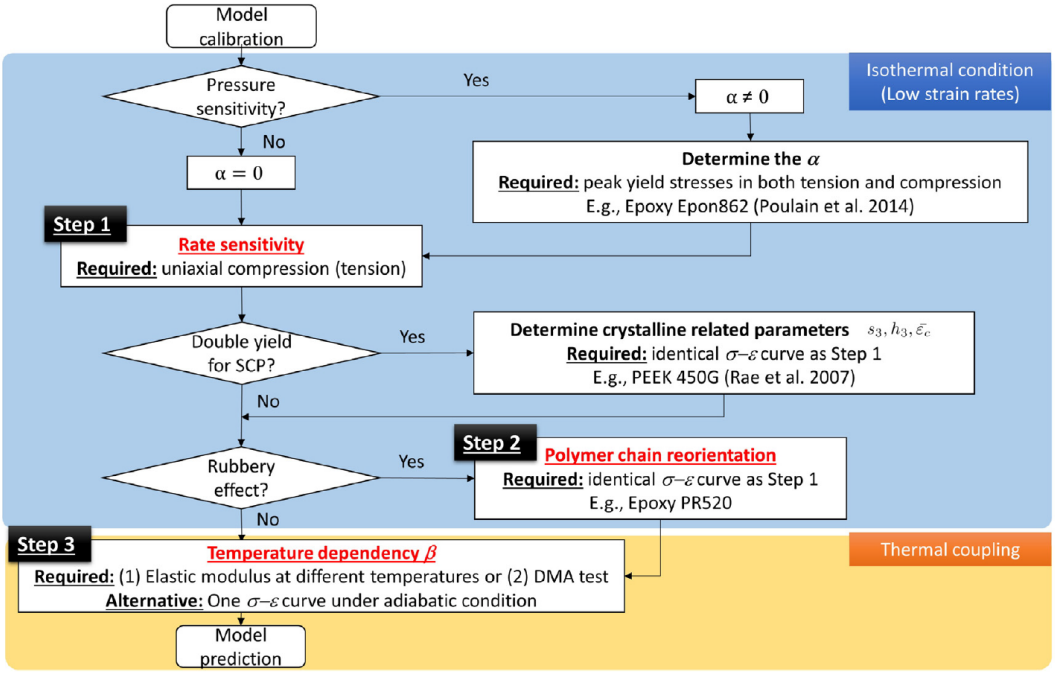

Fig. 15: Flowchart for parameter identification procedure using the USCP model [Hao et al., 2022b].

2.5.2 Example: ...

In their work, Hao et al. [2023] ...

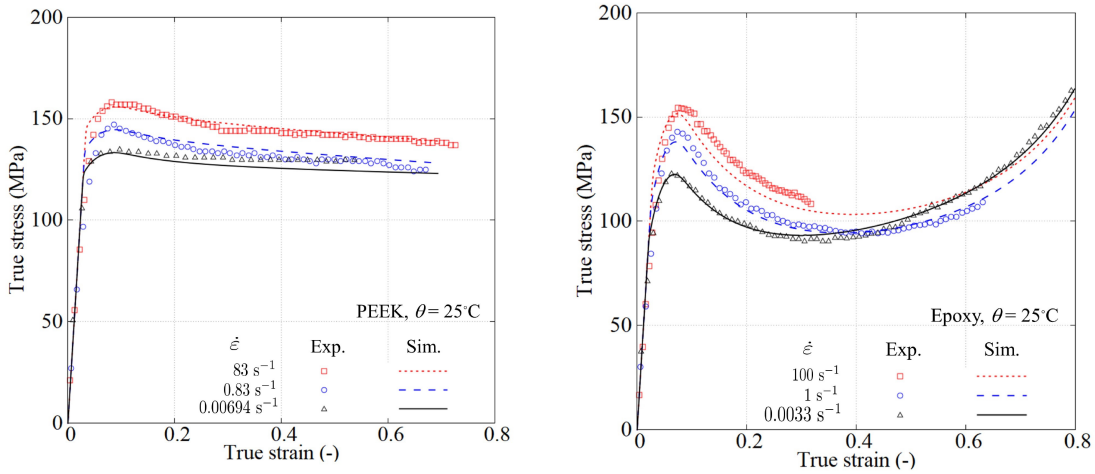

(a) **(b)**

Fig. 16: Comparison of experimental stress-strain curves at different strain rates with results using the USCP model for (a) KT880-NT PEEK and (b) PR520 epoxy resins [Hao et al., 2023].

A prominent strain softening is observed for the epoxy resin past peak yield. This may be interpreted as the internal structure changes in the glassy polymers, where polymer chains tend to reach their preferred saturated state [Hao et al., 2022b]. The nonlinear stress increase with a raised trend in the true stress-strain curve can be explained by the rubbery effect causing reorientation of the polymer chains Hao et al. [2022b]. This shows that, for epoxy, polymer chain reorientation dominates material behavior at large strain range. However, for PEEK, this

rubbery effect is not observed. This may be due to two reasons [Hao et al., 2022b]: (i) less capability of intrinsic polymer chain reorientation in PEEK, or (ii) the investigated strain range is not large enough. Therefore, the branch relative to network resistance may be dropped when modelling PEEK with the USCP model (i.e. no data in the table).

Material Parameter	Unit	PA6	PEEK	PR520	Description
Mechanical constants					
E_{ref}	GPa	2.62	4.33	4.28	Modulus at θ_{ref}
θ_{ref}	K	296	298	298	Reference temperature
ν	-	0.39	0.37	0.40	Poisson's ratio
β	1/K	0.0036	0.0007	0.0012	Temperature dependence
α	-	0	0	0	Pressure sensitivity
$\dot{\varepsilon}_0$	1/s	3.55×10^{11}	4.27×10^{4}	1.76×10^{9}	Rate sensitivity
m	-	0.83	0.66	0.66	Rate sensitivity
A	K/MPa	104	177.4	133.8	Rate sensitivity
s_0	MPa	184	161.6	172.3	Initial equivalent strength
s_1	MPa	196	174.8	242.5	Athermal peak strength
s_2	MPa	193	169.3	179.5	First saturation strength
s_3	MPa	234	-	-	Second saturation strength
h_1	MPa	32351	3747	6798	Pre-peak hardening
h_2	MPa	14827	959	635	Post-peak softening
h_3	MPa	681	-	-	Second yield hardening
$\bar{\varepsilon}_{\text{p}}$	-	0.009	0.0566	0.0407	Peak plastic strain
$\bar{\varepsilon}_{\text{c}}$	-	0.0295	-	-	Activation plastic strain
f	-	0.3	0.3	0.3	Smooth factor
C^R	MPa	-	-	13.5	Rubbery modulus
N	-	-	-	1.7	number of rigid links
Physical constants					
ρ	kg/m^3	1200	1300	1250	Density
k	W/m K	0.25	0.25	0.192	Thermal conductivity
c_{p}	J/kg K	1700	1330	1100	Specific heat

Fig. 17: Material parameters for the USCP model [Hao et al., 2023].

References

Argon, A.S., 1973. A theory for the low-temperature plastic deformation of glassy polymers. Philosophical Magazine 28, 839. doi:https://doi.org/10.1080/14786437308220987.

Arruda, E., 1992. Characterization of the strain hardening response of amorphous polymers. Ph.D. thesis. Massachusetts Institute of Technology, Dept. of Mechanical Engineering.

Arruda, E.M., Boyce, M.C., 1993. A three-dimensional constitutive model for the large stretch behavior of rubber elastic materials. Journal of the Mechanics and Physics of Solids 41, 389–412. doi:https://doi.org/10.1016/0022-5096(93)90013-6.

Bergström, J.S., 1999. Large Strain Time-Dependent Behavior of Elastomeric Materials. Ph.D. thesis. Massachusetts Institute of Technology, Dept. of Mechanical Engineering. doi:http://hdl.handle.net/1721.1/9794.

Bergström, J.S., 2015. Mechanics of Solid Polymers. William Andrew Publishing. doi:https://doi.org/10.1016/C2013-0-15493-1.

Bergström, J.S., Bischoff, J., 2010. An advanced thermomechanical constitutive model for uhmwpe. International Journal of Structural Changes in Solids 2, 31–39.

Bergström, J.S., Boyce, M.C., 1998. Constitutive modeling of the large strain time-dependent behavior of elastomers. Journal of the Mechanics and Physics of Solids 46, 931–954. doi:https://doi.org/10.1016/S0022-5096(97)00075-6.

Bergström, J.S., Boyce, M.C., 2000. Large strain time-dependent behavior of filled elastomers. Mech. Mater. 32, 620–644. doi:https://doi.org/10.1016/S0167-6636(00)00028-4.

Boyce, M.C., Arruda, E.M., 2000. Constitutive models of rubber elasticity: A review. Rubber Chemistry and Technology 73, 504–523. doi:https://doi.org/10.5254/1.3547602.

Boyce, M.C., Parks, D.M., Argon, A.S., 1988. Large inelastic deformation of glassy polymers. part i: rate dependent constitutive model. Mechanics of Materials 7, 15–33. doi:https://doi.org/10.1016/0167-6636(88)90003-8.

Boyce, M.C., Weber, G.G., Parks, D.M., 1989. On the kinematics of finite strain plasticity. J. Mech. Phys. Solids 37, 572–579. doi:https://doi.org/10.1016/0022-5096(89)90033-1.

Chowdhury, K.A., Talreja, R., Benzerga, A.A., 2008. Effects of manufacturing-induced voids on local failure in polymer-based composites. J. Eng. Mater. Technol. 130. doi:https://doi.org/10.1115/1.2841529.

Cohen, A., 1991. A padé approximant to the inverse langevin function. Rheol. Acta 30, 270–273. doi:https://doi.org/10.1007/BF00366640.

Courant, R., Friedrichs, K., Lewy, H., 1967. On the partial difference equations of mathematical physics. IBM Journal of Research and Development 11, 215–234. doi:https://doi.org/10.1147/rd.112.0215.

Dal, H., Kaliske, R., 2009. Bergström–Boyce model for nonlinear finite rubber viscoelasticity: theoretical aspects and algorithmic treatment for the FE method. Comput. Mech. 44, 809–823. doi:https://doi.org/10.1007/s00466-009-0407-2.

Gilabert, F.A., 2021. 8 - modelling nonlinear material response of polymer matrices used in fibre-reinforced composites, in: Van Paepegem, W. (Ed.), Multi-Scale Continuum Mechanics Modelling of Fibre-Reinforced Polymer Composites. Woodhead Publishing, pp. 219–242. doi:https://doi.org/10.1016/B978-0-12-818984-9.00008-1.

Gouhier, F., Diani, J., 2024. A comparison of finite strain viscoelastic models based on the multiplicative decomposition. European Journal of Mechanics - A/Solids 108, 105–424. doi:https://doi.org/10.1016/j.euromechsol.2024.105424.

Hao, P., Dai, Z., Laheri, V., Gilabert, F.A., 2022a. A unified amorphous-crystalline viscoplastic hardening law for non-isothermal modelling of thermoplastic and thermosets. International Journal of Plasticity

159, 103–469. doi:https://doi.org/10.1016/j.ijplas.2022.103469.

Hao, P., Spronk, S.W.F., Sevenois, R.D.B., Van Paepegem, W., Gilabert, F.A., 2023. Characterizing pure polymers under high speed compression for the micromechanical prediction of unidirectional composites. Polymers 15, 1262. doi:https://doi.org/10.3390/polym15051262.

Hao, P., Spronk, S.W.F., Van Paepegem, W., Gilabert, F.A., 2022b. Hydraulic-based testing and material modelling to investigate uniaxial compression of thermoset and thermoplastic polymers in quasistatic-to-dynamic regime. Materials & Design 224, 111–367. doi:https://doi.org/10.1016/j.matdes.2022.111367.

Jedynak, R., 2015. Approximation of the inverse langevin function revisited. Rheol. Acta 54, 29–39. doi:https://doi.org/10.1007/s00397-014-0802-2.

Korelc, J., Stupkiewicz, S., 2014. Closed-form matrix exponential and its application in finite-strain plasticity. International Journal for Numerical Methods in Engineering 98, 960–987. doi:https://doi.org/10.1002/nme.4653.

Kuhn, W., Grün, F., 1942. Beziehungen zwischen elastischen konstanten und dehnungsdoppelbrechung hochelastischer stoffe. Kolloid-Zeitschrift 101. doi:https://doi.org/10.1007/BF01793684.

Lee, E.H., 1969. Elastic-plastic deformation at finite strains. J. Appl. Mech. 36, 1–6. doi:https://doi.org/10.1115/1.3564580.

Platen, J., Pauls, B., Anantheswar, A., Lautenschläger, T., Neinhuis, C., Kaliske, M., 2024. A nonlinear finite viscoelastic formulation relative to the viscous intermediate configuration applied to plants. International Journal for Numerical Methods in Engineering 125, 74–83. doi:https://doi.org/10.1002/nme.7483.

Poulain, X., Benzerga, A.A., Goldberg, R.K., 2014. Finite-strain elasto-viscoplastic behavior of an epoxy resin: Experiments and modeling in the glassy regime. International Journal of Plasticity 62, 138–161. doi:https://doi.org/10.1016/j.ijplas.2014.07.002.

Reese, S., Govindjee, S., 1998. A theory of finite viscoelasticity and numerical aspects. International Journal of Solids and Structures 35, 3455–3482. doi:https://doi.org/10.1016/S0020-7683(97)00217-5.

Reif, F., 1965. Fundamentals of Statistical and Thermal Physics. Mc-Graw-Hill, New York.

de Souza Neto, E.A., Perić, D., J., O.D.R., 2008. B: The Tensor Exponential. John Wiley & Sons, Ltd. pp. 747–752. doi:https://doi.org/10.1002/9780470694626.app2.

Treloar, L.R.G., 1946. The elasticity of a network of long-chain molecules.—iii. Transactions of the Faraday Society 42. doi:https://doi.org/10.1039/TF9464200083.

Treloar, L.R.G., 1975. The Physics of Rubber Elasticity. Oxford University Press.

Wang, M.C., Guth, E., 1952. Statistical theory of networks of non-gaussian flexible chains. Journal of Chemical Physics 20, 1144–1157. doi:10.1063/1.1700682.

Weber, G., Anand, L., 1990. Finite deformation constitutive equations and a time integration procedure for isotropic, hyperelastic-viscoplastic solids. Computer Methods in Applied Mechanics and Engineering 79, 173–202. doi:https://doi.org/10.1016/0045-7825(90)90131-5.

Wu, P.D., van der Giessen, E., 1993. On neck propagation in amorphous glassy polymers under plane strain tension. International Journal of Plasticity 3, 211–235. doi:https://doi.org/10.1016/0749-6419(94)00043-3.